Comparisons of Turbulence Stresses from Experiments against the Attached Eddy Hypothesis in Boundary Layers.

R. Baidya, J. Philip, J. P. Monty, N. Hutchins and I. Marusic

Department of Mechanical Engineering
The University of Melbourne, Victoria 3010, Australia

Abstract

Turbulence stress statistics in a boundary layer at $Re_\tau \approx 10,000$ are measured using custom $\times$ hot-wire probes. The results show logarithmic behaviour in the profiles of the streamwise and spanwise turbulence intensities against wall-normal distance in the same region in which the mean velocity exhibits logarithmic behaviour, consistent with the predictions of the attached eddy hypothesis. Comparisons are drawn with computations applying the attached eddy hypothesis using two different typical representative eddies: (i) hierarchies of individual hairpins and (ii) hierarchies of packets of hairpins. Promising results are obtained when a packet-eddy is used rather than an individual hairpin-eddy, when compared with experimental results in the logarithmic region.

Introduction

In the attached eddy hypothesis, the turbulent boundary layer is idealised as a collection of randomly arranged geometrically similar representative eddies [11]. From this model, Townsend [11] concludes that at sufficiently high Re, the turbulence intensities follow

$$\frac{\overline{u^2}}{U_\tau^2} = -A_1 \ln \frac{z}{\delta} + B_1, \tag{1}$$

$$\frac{\overline{v^2}}{U_\tau^2} = -A_2 \ln \frac{z}{\delta} + B_2, \tag{2}$$

and

$$\frac{\overline{w^2}}{U_\tau^2} = B_3, \tag{3}$$

in the logarithmic region, assuming $\overline{uw}/U_\tau^2 = -1$, where U_τ corresponds to the friction velocity, while A_1, A_2, B_1, B_2 and B_3 are constants which depends on the form of the attached eddies. Throughout the paper, we use the co-ordinate system x, y and z to refer to the streamwise, spanwise and wall-normal directions; with u, v and w denoting the corresponding fluctuating velocities, respectively. Here we use the superscript '+' to indicate viscous scaled quantities, while capitalisation and overbars indicate time averaged quantities.

The representative eddies have characteristic heights ranging from δ_1, the smallest eddy, to Δ_E, the largest eddy of the order of the boundary layer thickness (δ). Eddies of identical characteristic height are referred to as a 'hierarchy', with multiple hierarchies representing various energetic scales present in the flow. Figures 1(a) and (b) show two examples of simple representative eddies (further details of the geometries are provided in a later section), while figures 1(c) and (d) show the idealised boundary layers with three hierarchies of representative eddy (i.e. δ_1 and Δ_E correspond to the characteristic heights of the first and third hierarchy, respectively). It should be noted that the representative eddy is a statistical concept which captures the bulk features of the average eddy shape. In reality, the shape and size of eddies evolve over their life span and hence it is highly unlikely
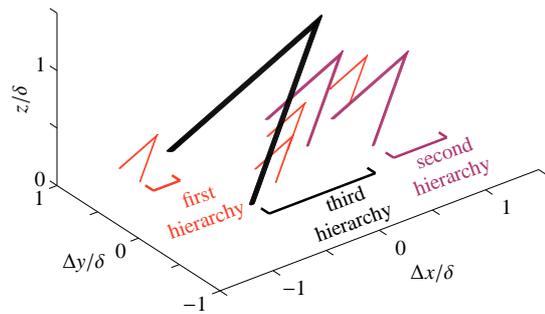
(a) Hairpin-eddy
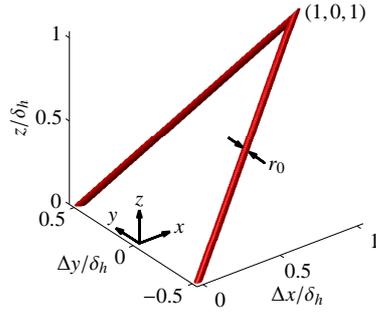
(b) Packet-eddy
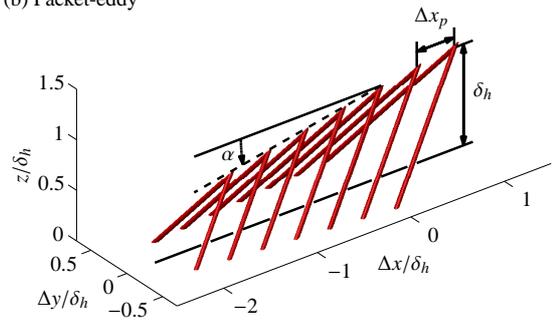
(c) Hierarchies of hairpin-eddy
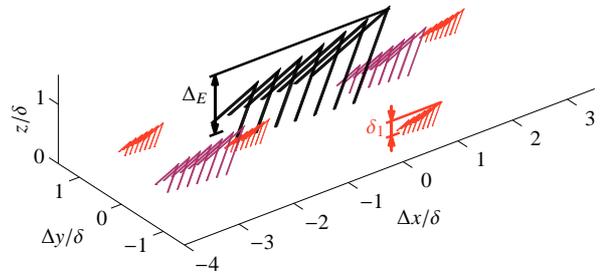

(d) Hierarchies of packet-eddy

Figure 1. Representative eddy constructed from (a) a single hairpin vortex and (b) multiple (seven) hairpin vortices in a packet. $r_0/\delta_h = 0.02$, $\alpha = 10°$, $\Delta x_p/\delta_h = 0.4$ in the present analysis. (c) and (d): Idealisation of a boundary layer composed of three hierarchies of the representative eddies shown in (a) and (b), respectively. It should be noted that, the streamwise and spanwise coordinates are shown here are relative ($\Delta x, \Delta y$) to an arbitrary position.

that they would instantaneously resemble the ensemble-averaged form. For example, there is evidence suggesting that instantaneously, vortices can be cane like with a single leg extending to the wall [3] rather than the idealised hairpin type employed here with both legs extending to the wall. However, since the likelihood of the cane vortices containing a leg with the opposing sign is equal [3], the resulting ensemble-average view will be very similar to that of a hairpin.

The initial attached eddy model of Perry *et al.* [8, 9] employed hierarchies of Λ shaped vortices. Perry *et al.* [9] report that the results from this model show a qualitative agreement with the experimental results. Marusic [5] refined the model of Perry *et al.* such that the representative eddy is formed from multiple hairpin vortices, rather than a single hairpin vortex. The multiple vortices align in the streamwise direction, similar to the 'packet' paradigm proposed by Adrian *et al.* [1]. Marusic found that the subsequent two-point correlation results from hierarchies of the packet-eddy are in a better agreement with the experimental data than those obtained using a single hairpin as the representative eddy [5].

Here, we compare the turbulence intensities of all three components and the Reynolds shear stress from the attached eddy hypothesis against experimental data. A link between the representative eddies used in the attached eddy hypothesis and the slope of the logarithmic behaviour in $\overline{u^2}$ and $\overline{v^2}$ is explored.

Experimental Set-up

The experiments are conducted in the High Reynolds Number Boundary Layer Wind Tunnel (HRNBLWT), located at the University of Melbourne. This is an open-return blower tunnel with a long working section (27 m), which allows a boundary layer with a thickness of up to 0.35 m to be developed. This enables the development of high Reynolds number (Re) boundary layers at relatively low freestream velocities. The key advantage of this approach is that the smallest energetic length and time scales are accessible with conventional measurement techniques. For example, at $Re_\tau \approx 10,000$ the viscous length and time scales correspond to approximately $30\,\mu m$ and $60\,\mu s$, respectively.

Two hot-wires in an '$\times$' arrangement are used to measure the u, v and w velocities. As the $\times$-probe can only measure two velocity components simultaneously, the u, v and w statistics presented here have been compiled from two separate profiles taken using two different $\times$-probe configurations. All the $\times$-probes are custom made in-house. A schematic highlighting key features is given in figure 2(a). The $\times$ formed by the two hot-wires defines a box with dimensions 0.4×0.4 mm (14×14 wall units) and a wire spacing of 0.2 mm ($\Delta s^+ = 7$) as shown in figures figure 2(b) and (c). These probes are significantly more spatially compact than commercially available alternatives. The probes are manufactured such that the sensing elements remain parallel to the wall when the probe body is inclined at $10°$ to the horizontal (this inclination is shown in figure 2a), allowing access close to the wall while also minimising aerodynamic blockage effects.

The prongs of the custom probe are constructed from four $250\,\mu m$ diameter stainless steel wires held together by epoxy resins. The prong tips are sharpened down to $20\,\mu m$, and a thin layer ($< 10\,\mu m$) of copper is deposited via electrolysis. The copper-plating significantly improves solderability of the prong tips, allowing $2.5\,\mu m$ diameter platinum wires to be soldered to them. Further details of the custom probe and the calibration procedure employed is given by Baidya *et al.* [2].

The measurements are conducted at approximately 18 m downstream of the tripped inlet of the working section with a nominal freestream velocity of 15 m/s, which corresponds to $Re_\tau \approx$
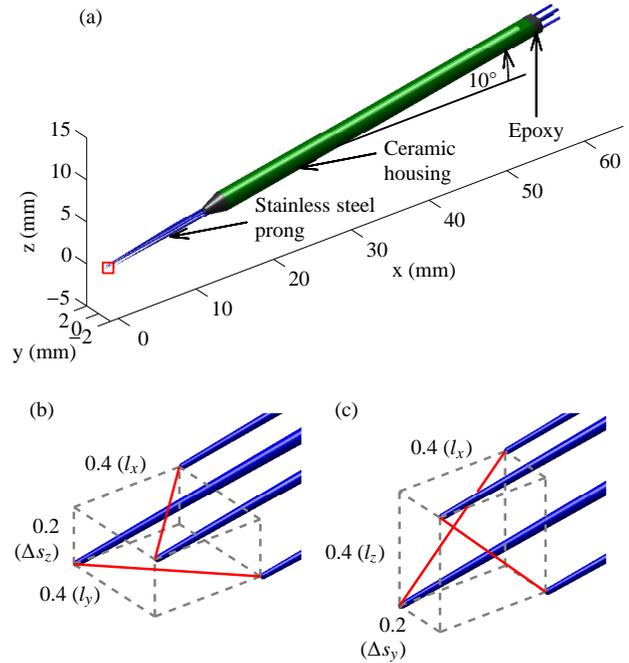

Figure 2. Schematic of the custom $\times$-wire probe (all dimensions in mm). (a) Probe at designed orientation for boundary layer measurements. The region in the square box is enlarged for (b) *u-v* measurement configuration and (c) *u-w* measurement configuration, with the $0.4 \times 0.4 \times 0.2$ mm cuboid volume that encapsulates the sensors shown by the dashed lines. The platinum sensing elements are shown as solid red lines in (b) and (c).

10,000, under nominally zero pressure gradient conditions. The boundary layer thickness and friction velocity have been obtained by fitting the mean velocity profile to the composite formulation of Chauhan *et al.* [4] yielding $\delta = 0.33$ m and $U_\tau = 0.48$ m/s, respectively.

Attached Eddy Formulation

In this section, we outline how the turbulence stress profiles are determined following the attached eddy formulation. In the present analysis, we use hierarchies of hairpin- and packet-eddies to construct the turbulence stress profiles. Throughout, we use a Λ vortex as the model for a hairpin, similar to the work of Perry *et al.* [8]. The Λ vortex has an inclination angle of $45°$ with respect to the x direction. Figure 1(a) shows a schematic of the Λ hairpin-eddy used in this study. For the packet-eddy, seven Λ vortices each separated by $0.4\delta_h$ in the x direction are used. Here, δ_h corresponds to the characteristic height of the largest hairpin in the packet. The height of each Λ vortex is adjusted so that the heads are aligned in the x direction with a characteristic angle of $10°$, mimicking experimental observations [1]. Figure 1(b) shows the hairpin alignment used to construct the packet-eddy. It should be noted that to preserve the no-penetration condition at the wall, each vortex rod is supplemented with a corresponding mirror image about the wall.

As the representative eddies across the hierarchies are randomly aligned in the attached eddy model, the turbulence stresses from multiple hierarchies can be calculated solely using the basis functions I_{ij} obtained from a single representative eddy following Campbell's theorem. The Townsend eddy-intensity function, I_{ij} is given by

$$I_{ij}\left(\frac{z}{\delta_h}\right) = \int_{-\infty}^{\infty}\int_{-\infty}^{\infty} \frac{u_i}{U_0}\frac{u_j}{U_0} \, d\left(\frac{x}{\delta_h}\right) d\left(\frac{y}{\delta_h}\right), \quad (4)$$

where u_i and u_j are the induced fluctuating velocities due to the representative eddy, while U_0 denote the characteristic velocity scale.
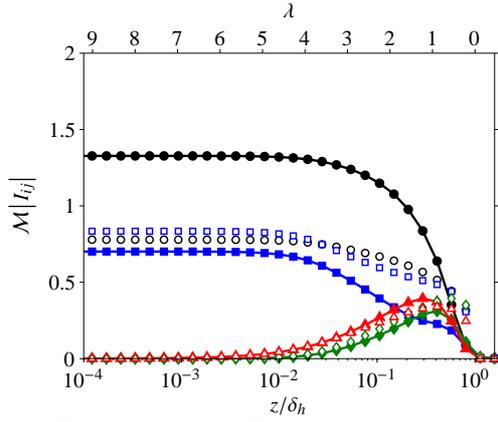
Figure 3. Comparison between Townsend eddy-intensity functions for hairpin- (empty symbols) and packet (solid symbols) representative eddies constructed using Λ shaped vortices. The symbols correspond to: $\bigcirc$ I_{11}, $\square$ I_{22}, $\diamond$ I_{33} and $\triangle$ $-I_{13}$.
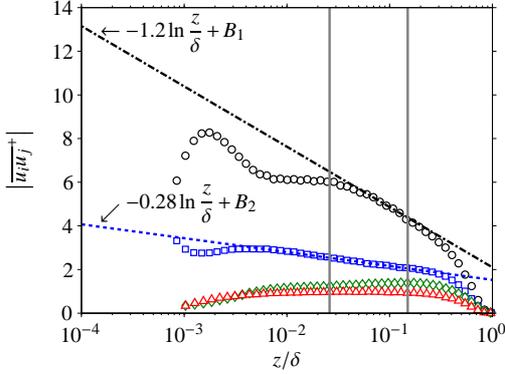

Figure 4. Turbulence stresses determined experimentally, at $Re_\tau \approx 10,000$. The symbols correspond to: $\bigcirc$ $\overline{u^2}$, $\square$ $\overline{v^2}$, $\diamond$ $\overline{w^2}$ and $\triangle$ $-\overline{uw}$, while the dot-dashed and dotted line represent the logarithmic law fitted to $\overline{u^2}$ and $\overline{v^2}$, respectively. The vertical lines corresponds to locations $z^+ = 2.6\sqrt{\delta^+}$ and $z^+ = 0.15\delta^+$.

The turbulence stress distribution from multiple hierarchies of geometrically similar eddies can be calculated using

$$\frac{\overline{u_i u_j}}{U_\tau^2} = \int_{\delta_1}^{\Delta_E} I_{ij}\left(\frac{z}{\delta_h}\right) p_H(\delta_h)\, d\delta_h, \qquad (5)$$

where $p_H(\delta_h)$ is the p.d.f of hierarchy scales. Empirically, it is known that for large Re $-\overline{uw}^+$ approaches unity, hence for the attached eddy formulation we select U_0 such that $-\overline{uw}_{\text{peak}}/U_0^2 = 1$ and take U_0 as U_τ for our finite but relatively high Re cases.

We follow the approach of Townsend [11] and assume $p_H(\delta_h) = 1/\delta_h$. The $1/\delta_h$ distribution implies a doubling of the representative eddy density as the characteristic height halves. Perry at al. [8] hypothesise that jitter introduced by randomness leads to a continuous distribution rather than a discrete geometric distribution of scales. It should be noted that equation (5) is marginally different from Perry *et al.* [7], where an additional weighting term $Q(\delta_h/\Delta_E)$ is present to account for non-uniformity in the vorticity distribution across the hierarchies. In the present analysis, the vorticity distribution across the hierarchies is considered to be uniform and hence $Q = 1$. It should be noted that the $1/\delta_h$ distribution is a simplified view of a boundary layer, which in reality is far more complex. However, the simplified model still manages to capture the logarithmic behaviour of U and $\overline{uw} \simeq$ constant and hence is a useful idealisation of the log region. Perry at al. [8, 9] propose modifying the $p_H(\delta_h)$ distribution to obtain the correct mean velocity profile in the buffer and wake regions. However, for the present analysis we are only interested in the log region and hence have used the form proposed
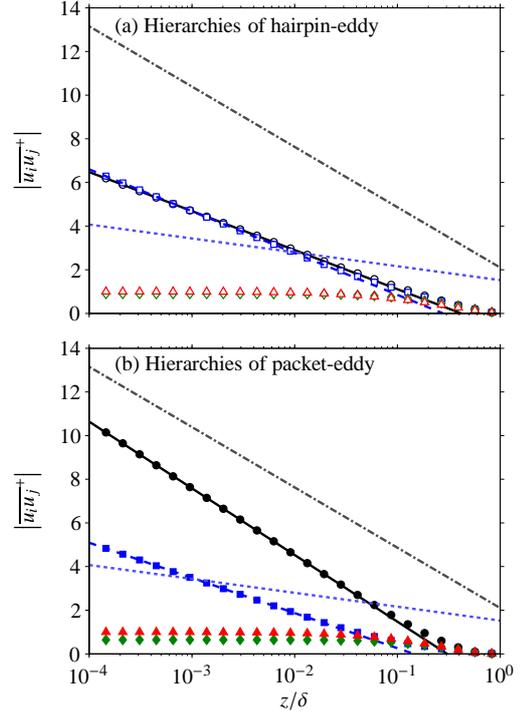
by Townsend. It has also been suggested that different representative eddies may be required to model the wake region [7]. Again, this modification is not required here, where we only seek to model the logarithmic region.

Equation (5) can be rewritten in the logarithmic form as

$$\frac{\overline{u_i u_j}}{U_\tau^2} = \int_{\lambda_1}^{\lambda_E} I_{ij}(\lambda)\, w(\lambda - \lambda_E)\, d\lambda, \qquad (6)$$

where $\lambda = \ln(\delta_h/z)$, $\lambda_1 = \ln(\delta_1/z)$ and $\lambda_E = \ln(\Delta_E/z)$. The weighting function $w(\lambda - \lambda_E) = 1$ for the $1/\delta_h$ distribution of hierarchies used in the present study.

Results

Figure 3 shows the normalised eddy-intensity functions for the hairpin- and packet representative eddy. It is evident that as z/δ_h decreases, I_{11} and I_{22} approach a constant while I_{33} and I_{13} approach zero since $u \neq 0$, $v \neq 0$ and $w = 0$ at the wall. The normalisation factor $\mathcal{M}$ is chosen so that

$$\mathcal{M} \int_0^\infty I_{13}(\lambda)\, d\lambda = -1. \qquad (7)$$

It follows then that the constants given in equations (1) - (3) can be related to the functions as:

$$A_1 = \mathcal{M} I_{11}(\lambda = \infty), \qquad (8)$$
$$A_2 = \mathcal{M} I_{22}(\lambda = \infty), \qquad (9)$$

and

$$B_3 = \mathcal{M} \int_0^\infty I_{33}(\lambda)\, d\lambda, \qquad (10)$$

as given by Perry at al. [9]. Figure 3 indicates that for $z/\delta_h \leq 10^{-3}$ ($\lambda \gtrsim 7$), the eddy-intensity functions have sufficiently approached the corresponding asymptotic values. This implies that

Figure 5. Turbulence stresses following the attached eddy hypothesis. The symbols correspond to: $\bigcirc$ $\overline{u^2}$, $\square$ $\overline{v^2}$, $\diamond$ $\overline{w^2}$ and $\triangle$ $-\overline{uw}$. Representative eddy constructed using (a) a single Λ vortex and (b) a packet of multiple Λ vortices. Solid lines indicate the logarithmic fit for $\overline{u^2}$, while dashed lines indicate the logarithmic fit for $\overline{v^2}$. The logarithmic law determined from experiments, shown in figure 4 is replicated for reference.

$\delta_1/\Delta_E = 10^{-3}$ is sufficiently close to the asymptotical state, since $\overline{u_i u_j}_{\text{peak}} \approx \int_0^\infty I_{13}\, d\lambda$ for $\delta_1/\Delta_E \leq 10^{-3}$.

In the near-wall region, the velocity contribution from the hairpin legs dominates due to the hairpin legs' proximity to the wall and hence the value of I_{11} and I_{22} at the wall is primarily due to the geometry of the hairpin leg. A low streamwise momentum region exists between the legs of hairpin vortices, while each leg is flanked by elongated regions of low and high v. Hence, in a packet-eddy, u contributions from each vortex overlap and combine, while v contributions from each vortex remain isolated with little overlap between adjacent vortices. Hence, I_{22} at $z/\delta_h = 0$ scales approximately with the number of hairpins in the packet while I_{11} at $z/\delta_h = 0$ does not. Although the area under the $\mathcal{M}I_{13}$ curve is adjusted to equal -1, the uw contribution for the packet-eddy is concentrated at a lower wall position compared to the individual hairpin-eddy. This is because the hairpin heads form a characteristic angle of $10°$ in the packet-eddy and hence a higher proportion of uw containing motions are at a lower z compared to the hairpin-eddy.

The experimental data provide evidence of the logarithmic behaviour in $\overline{u^2}$ and $\overline{v^2}$, as predicted by equations (1) and (2) and are shown in figure 4. The value for the gradient in equation (1), $A_1 \approx 1.2$ reported by Marusic $et\ al.$ [6] is in good agreement with the current data, while $A_2 \approx 0.28$ is obtained based on a linear regression in the region $2.6\sqrt{\delta^+} < z^+ < 0.15\delta^+$. Comparison with the $\overline{v^2}$ profile obtained from Direct Numerical Simulation (DNS) of a developing boundary layer [10] shows good agreement, albeit at low Re. A survey of A_2 in the pipe, channel and boundary layer DNSs at $Re_\tau \approx 2{,}000$ reveals that the logarithmic behaviour of $\overline{v^2}$ in the boundary layer is much shallower than that observed in the pipe and channel, where both exhibit $A_2 \approx 0.5$. For $\overline{w^2}$ the experimental data show a slight increase with z in the log region, where the attached eddy model predicts constant stress (see equation 3). However, this may be explained by more energetic high-wavenumber viscous motions associated with Kolmogorov inertial subrange and dissipative range at a higher z position observed to occur at a finite Re [7], which is not accounted for in the attached eddy model.

Figure 5(a) and (b) show the corresponding $\overline{u_i u_j}$ profiles following the attached eddy hypothesis. When hierarchies of hairpin-eddies are used (ref. figure 5a), the slope of the logarithmic region for both $\overline{u^2}$ and $\overline{v^2}$ is similar with $A_1 \approx A_2 \approx 0.9$ for this particular hairpin-eddy geometry. Hence, the value of A_1 is underestimated while the value of A_2 is overestimated when compared with the experimental data. When hierarchies of packet-eddies are used instead of the individual hairpin-eddy, the value of A_1 increases while the value of A_2 decreases (ref. figure 5b). As discussed earlier, u contributions from multiple aligned vortices superimpose, resulting in a significant increase in the maximum u deviation occurring within the packet-eddy. A similar mechanism applies to w but with a smaller magnitude, while v contributions are isolated and the maximum deviation does not change significantly with the form of the representative eddy. Hence $\Delta I_{11} > \Delta I_{13} > \Delta I_{22}$, where Δ signifies the difference between the eddy-intensity functions for the packet- and hairpin representative eddies. This leads to an increase in A_1 and a decrease in A_2 when I_{13} is normalised to be equal to -1, a trend that is more consistent with the experimental data.

Summary and Conclusions

Experimental data for a zero pressure gradient boundary layer at $Re_\tau \approx 10{,}000$ show a logarithmic behaviour for the $\overline{u^2}$ and $\overline{v^2}$ statistics, in agreement with the attached eddy hypothesis. A weak relationship between $\overline{w^2}$ and z is observed experimentally in the log region, in contrast to the constant value predicted by the attached eddy hypothesis. The departure of $\overline{w^2}$ from the constant value may be attributed to finite Re effects, which results in contribution from high-wavenumber motions differing with the z position [7].

The experimental turbulence stress profiles are compared with the profiles from hierarchies of hairpin- and packet-eddies obtained from the attached eddy hypothesis. The profiles from hierarchies of hairpin-eddies underestimate the slope of the logarithmic law in $\overline{u^2}$, while the slope of $\overline{v^2}$ is over estimated. Improved results are obtained using hierarchies of packet-eddies, where an increase in the slope of the logarithmic law in $\overline{u^2}$ is observed as well as a decrease in the slope in $\overline{v^2}$. Therefore, the packet scenario is a better idealisation of the representative attached eddy for the logarithmic region of wall turbulence compared to an individual vortex structure. These results are based on the simplest constructions of representative eddies, and further refinement would be needed to obtain more precise quantitative predictions. The trends, however, (packet versus individual eddies) are not expected to be different.

References

[1] Adrian, R. J., Meinhart, C. D. and Tomkins, C. D., Vortex organization in the outer region of the turbulent boundary layer, *J. Fluid Mech.*, **422**, 2000, 1–54.

[2] Baidya, R., Philip, J., Hutchins, N., Monty, J. P. and Marusic, I., Measurements of streamwise and spanwise fluctuating velocity components in a high Reynolds number turbulent boundary layer, in *Proceedings of 18th Australasian Fluid Mechanics Conference*, 2012.

[3] Carlier, J. and Stanislas, M., Experimental study of eddy structures in a turbulent boundary layer using particle image velocimetry, *J. Fluid Mech.*, **535**, 2005, 143–188.

[4] Chauhan, K. A., Monkewitz, P. A. and Nagib, H. M., Criteria for assessing experiments in zero pressure gradient boundary layers, *Fluid Dyn. Res.*, **41**, 2009, 021404.

[5] Marusic, I., On the role of large-scale structures in wall turbulence, *Phy. Fluids*, **13**, 2001, 735–743.

[6] Marusic, I., Monty, J. P., Hultmark, M. and Smits, A. J., On the logarithmic region in wall turbulence, *J. Fluid Mech.*, **716**, 2013, 716.

[7] Perry, A. and Marusic, I., A wall-wake model for the turbulence structure of boundary layers. Part 1. Extension of the attached eddy hypothesis, *J. Fluid Mech.*, **298**, 1995, 361–388.

[8] Perry, A. E. and Chong, M. S., On the mechanism of wall turbulence, *J. Fluid Mech.*, **119**, 1982, 173–217.

[9] Perry, A. E., Henbest, S. and Chong, M. S., A theoretical and experimental study of wall turbulence, *J. Fluid Mech.*, **165**, 1986, 163–199.

[10] Sillero, J. A., Jiménez, J. and Moser, R. D., One-point statistics for turbulent wall-bounded flows at Reynolds numbers up to $\delta^+ \approx 2000$, *Phy. Fluids*, **25**, 2013, 105102.

[11] Townsend, A. A., *The structure of turbulent shear flow*, Cambridge University Press, Cambridge, UK, 1976.